CrossMark

Axial Load Testing of Hybrid Concrete Columns Consisting of UHPFRC Tube and Normal-Strength Concrete Core

Xiangguo Wu[1,2], Thomas H.-K. Kang[3], Issa Brown Mpalla[1], and Chang-Soo Kim[4],*

Abstract: To investigate the axial load behavior of hybrid concrete columns consisting of an ultra-high performance fiber-reinforced concrete tube (20 mm thick, 92.6 MPa or 143.3 MPa) and normal-strength concrete core (28.2 MPa), concentric axial load tests were performed for five column specimens. The UHPFRC tube can function as a form during core-filling and as a cover having high performance at service and ultimate load conditions. Axial loading was applied to the core only, and the tube was indirectly loaded by bearing of transverse threaded bars. Test parameters included the volume fraction of steel fibers, volumetric ratio of transverse bars, and usage of wire-mesh in the tube. Test results showed that structural performance such as initial stiffness, peak load, displacement ductility, and energy absorption capacity varied greatly according to each test parameter. During the course of axial loading applied on the core only, the axial load behavior of the hybrid concrete columns generally corresponded to the full composite action at the initial loading stage and then changed to that of non-composite action (core only) after the failure of the threaded bars.

Keywords: hybrid concrete column, UHPFRC tube, normal-strength concrete core, concentric axial load test.

1. Introduction

Ultra-high performance fiber-reinforced concrete (UHPFRC) is a type of fiber-reinforced cementitious composites having advantages of very high strength (both in compression and tension), toughness, and durability (Mehta and Monteiro 2006). The use of UHPFRC has gained widespread acceptance in the construction industry over the past two decades. Although there are still competing approaches to obtain an optimized mechanical behavior (Mehta and Monteiro 2006), according to the French Association for Civil Engineering (AFGC) (Toutlemonde et al. 2000; Toutlemonde and Resplendino 2011), UHPFRC with a compressive strength of 150 MPa or greater is now commercially available by careful selection/control of material compositions, mixing methods, equipment, placing procedures, and curing process.

As a construction material, UHPFRC has a high potential for newer applications, because of the following superior performance under harsh environments: high impermeability against moisture or other chemicals, high mechanical resistance to corrosion and abrasion, and high physical resistance to impact (Mirmiran and Mohsen 1997; Foster and Mario 2001; Neves and Fernandes de Almeida 2005; Pimienta and Chanvillard 2005; Mehta and Monteiro 2006; Fehling et al. 2008; Paultre et al. 2010; Toutlemonde and Resplendino 2011; Nematollahi et al. 2012; Park et al. 2016). This is possible because of the dense microstructure associated with steel fibers. Further advantages of UHPFRC include the low probability of cracking, high modulus of elasticity, early removal of concrete formwork, and high load-carrying and energy absorption capacity.

One common application of UHPFRC is found in vertical elements of tall buildings, because UHPFRC enables columns to have a smaller cross-section. Using the hybrid application of placing UHPFRC only in the perimeter of a cross-section is relatively economical. Having different strength concretes for the cover and core is structurally efficient and cost-effective. Concrete cover provides the protection of structural steel and reinforcement against corrosion and fire (ACI 318-14 2014), but early spalling of the concrete cover may occur due to shrinkage effects and weakness of planes between the concrete

[1]Key Lab of Structures Dynamic Behavior and Control of the Ministry of Education and School of Civil Engineering at Harbin Institute of Technology, 92 West Dazhi Street, Nan Gang District, Harbin 150001, Heilongjiang, China.
[2]Key Lab of Smart Prevention and Mitigation of Civil Engineering Disasters of the Ministry of Industry and Information Technology, Harbin Institute of Technology, Harbin 150090, China.

[3]Department of Architecture and Architectural Engineering, Seoul National University, 1 Gwanak-ro, Gwanak-gu, Seoul 08826, South Korea.

[4]School of Civil Engineering at Shandong Jianzhu University and Shandong Provincial Key Laboratory of Appraisal and Retrofitting in Building Structures, Fengming Road, Lingang Development Zone, Jinan 250101, Shandong, China.
*Corresponding Author; E-mail: mukan05@snu.ac.kr

cover and core (bounded by longitudinal and transverse bars) (Collins et al. 1993; Cusson and Paultre 1994). This phenomenon becomes more obvious when higher strength concrete and denser reinforcement are used (Collins et al. 1993; Cusson and Paultre 1994). In particular, the confinement effect of transverse bars, which is critical in the design of columns, is not fully developed until a column is subjected to sufficient compression and deformation, and the large compression and deformation lead to cover-spalling (ACI 318-14). However, in the case of using UHPFRC for the cover, the cover-spalling can be much retarded. Thus, the UHPFRC cover (or tube), which can also act as a light and durable permanent form, can improve the efficiencies of hybrid concrete columns (HCC). Similar types of columns can be seen in the strengthening of existing columns (Wang and Lee 2007; Tsonos 2009; Koo et al. 2016) and in the construction of concrete-filled hollow precast concrete columns (Kim et al. 2016, 2017) (Fig. 1). The perimeter tube section could be either loaded (directly or indirectly) or unloaded (confinement only) depending on the details of tube-core interfaces. Although there are several existing studies on the behavior of UHPFRC columns, in most of them UHPFRC is used for the whole section and only a few studies are available for hybrid UHPFRC columns.

In the present study, a thin tube (20 mm) of UHPFRC was used as the perimeter cover, which was indirectly loaded by bearing of transverse threaded bars, and the core was filled with normal-strength concrete (NSC), which was directly loaded. To investigate the effect of the UHPFRC tube with various parameters, concentric axial load tests were performed for five HCC columns.

2. Test Plan

2.1 Test Specimens

To evaluate structural performance and applicability, concentric axial load tests were performed for five HCC specimens consisting of a UHPFRC tube and NSC core. Test parameters included the volume fraction (V_f) of steel fibers, volumetric ratio (ρ_{st}) of transverse bars, and usage of wire-mesh. Figure 2 shows the configuration and dimensions, and Table 1 summarizes the test parameters.

All the column specimens had a square cross-section of 400×400 mm and a length of 1200 mm. The wall thickness of the UHPFRC tube was 20 mm, and four 22 mm-diameter deformed bars were used for longitudinal reinforcement (reinforcement ratio $\rho = 1\%$). The UHPFRC tube of each specimen was built with a particular set of the test parameters. In the control specimen HCC1, the fiber volume fraction was $V_f = 1.5\%$, 10 mm-diameter transverse deformed bars were provided at a vertical spacing of $s = 100$ mm ($\rho_{st} = 2.52\%$), and 8 mm-aperture wire-mesh (woven by 0.8 mm-diameter wires of ordinary low carbon steel Q235) was used to improve the structural integrity of four sides of the UHPFRC tube. Next, V_f was increased to 2.0% in HCC2, while s was increased to 200 mm ($\rho_{st} = 1.26\%$) in HCC3. In HCC4, both V_f and s were increased to 2.0% and 200 mm, respectively, to investigate the combined effect of the greater fiber fraction and lower transverse bar ratio. HCC5 was the same as HCC1, except that wire-mesh was not used. For all specimens, 16 mm-diameter threaded bars were placed at a spacing of 200 mm before the core of the UHPFRC tube was filled with NSC. Since the threaded bars can act as form-ties for the thin-walled tube during core-filling, the spacing was determined considering formwork-pressure (Kim et al. 2016). The threaded bars (embedded through the UHPFRC tube and NSC core) also can act as shear-keys for bond between the UHPFRC tube and NSC core when subjected to load. The transverse bars and threaded bars were more closely spaced at column ends to prevent local failure that may occur accidentally during testing.

2.2 Material Properties
2.2.1 Concrete Mixes and Mechanical Properties

For UHPFRC, Grade 42.5 ordinary Portland cement was used. Silica fumes were used to partially replace cements, and silica flours were used as fillers (Shanmugapriya and
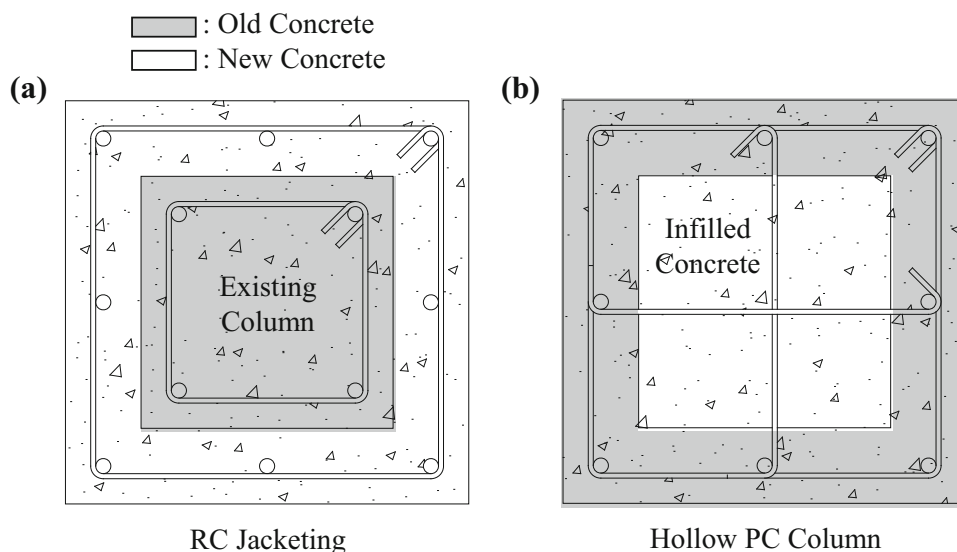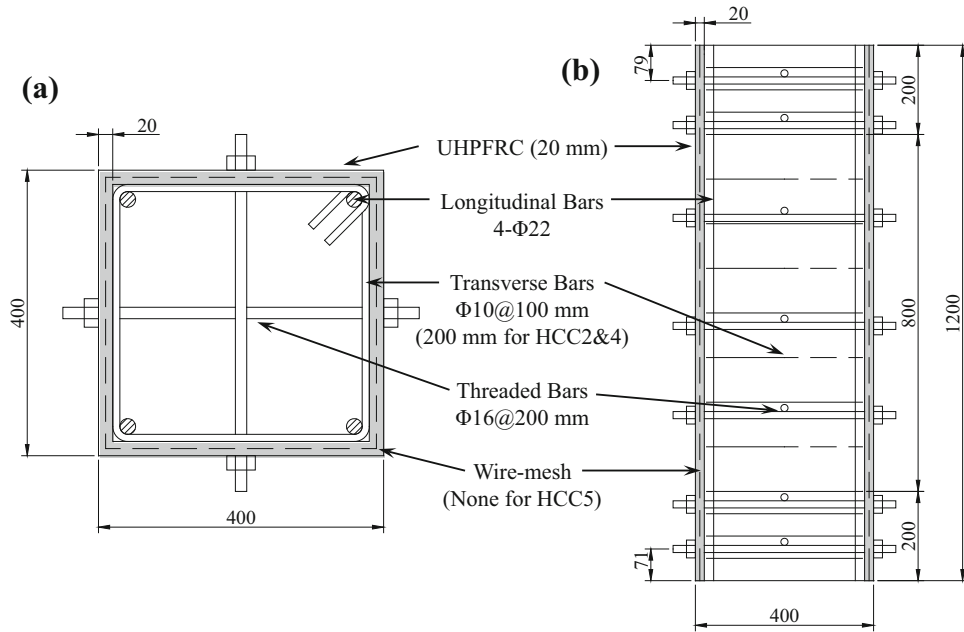

: Old Concrete
: New Concrete

(a) RC Jacketing

Existing Column

(b) Hollow PC Column

Infilled Concrete

Fig. 1 Example of hybrid concrete columns: **a** strengthening of existing column and **b** concrete-filled hollow PC column.

Fig. 2 Details of column specimens (units: mm): **a** cross-section and **b** elevation.

Table 1 Test parameters of column specimens.

Specimen	Fiber volume fraction, V_f (%)	Spacing of transverse bars, s (volumetric ratio, ρ_{st})	Wire-mesh
HCC1	1.5	100 mm (2.52%)	O
HCC2	2.0	100 mm (2.52%)	O
HCC3	1.5	200 mm (1.26%)	O
HCC4	2.0	200 mm (1.26%)	O
HCC5	1.5	100 mm (2.52%)	–

Cross-section = 400 × 400 mm, column length = 1200 mm, thickness of UHPFRC tube = 20 mm, longitudinal reinforcement = four 22 mm-diameter deformed bars (ρ = 1%), diameter of transverse bars = 10 mm, and threaded bars = 16 mm at a spacing of 200 mm.

Uma 2013). Washed river sands with fractions of 0–2 mm were used as fine aggregates, and no coarse aggregates (or gravel) were provided. The aspect ratio (ℓ_f/d_f, where fiber length $\ell_f = 13$ mm and fiber diameter $d_f = 0.2$ mm) and tensile strength (f_{fu}) of straight steel fibers were 65 and 2500 MPa, respectively. To achieve workable mixes with desired quality and strength, super-plasticizer and other chemical admixtures (expansive agent and deforming agent) were added in the form of aqueous solution with a small amount of water.

Table 2 presents the weight of materials per unit volume (kg/m³) for two UHPFRC mixes. The two UHPFRC mixes differed in the steel fiber content, and all the materials of both mixes were treated/controlled under the same conditions. Since the UHPFRC contained more constituents and finer particles than NSC and also included short and high-strength steel fibers, careful mixing was required to achieve proper workability, particle distribution, and packing density. In the present study, according to the recommendations of AFGC (2002) and FHWA-HRT-06-103 (Graybeal 2006), all fine dry particles were mixed first before adding the water and chemical admixtures: (1) the cements, silica fumes,

silica flours, and sands were dry-mixed for the first 5–10 min; (2) the water premixed with chemical admixtures was added slowly and continuously, and then the wet mixture was mixed again for another 5–10 min; and (3) when the mortar mixture showed enough fluidity to be workable and viscose for uniform fiber distribution, steel fibers were carefully introduced into the mixture by hand.

To investigate the mechanical properties of UHPFRC, according to GB/T 50081-2002 (2002), JSCE (2008), and ASTM C109-11 (2011), compression tests for 100 mm cubes and uniaxial tension tests for wire-meshed and notched dog-bone specimens (thickness × width × length of reduced section = 20 × 150 × 190 mm) were performed. Figure 3(a) shows the compressive stress–strain relationship of the cubes. As shown in the figure, the compressive stress linearly increased up to peak stress. Even though the post-peak behavior was not fully measured due to damage of strain-gauges, it was not brittle. The linear-elastic ascending and non-brittle descending behavior were attributed to finely graded and tightly packed materials and steel fibers (Graybeal and Hartmann 2003). The average 28 day cube strength (f_{cu}) and modulus of elasticity (E_c = secant modulus at

Table 2 Mix design of UHPFRC.

Mix type	1.5% V_f UHPFRC	2.0% V_f UHPFRC
Portland cement	769.8 kg/m³	766.9 kg/m³
Silica fume	192.5 kg/m³	191.7 kg/m³
Silica flour	231.0 kg/m³	230.1 kg/m³
Find sand	846.8 kg/m³	843.6 kg/m³
Super-plasticizer	30.8 kg/m³	30.7 kg/m³
Expansive agent	3.8 kg/m³	3.8 kg/m³
Deforming agent	3.8 kg/m³	3.8 kg/m³
Steel fibers	89.5 kg/m³	118.9 kg/m³
Water (W/B)[a]	192.5 kg/m³	191.7 kg/m³
	(0.2)	(0.2)

[a]W water, and B binders including cements and silica fumes (silica flours were considered as a filling material).
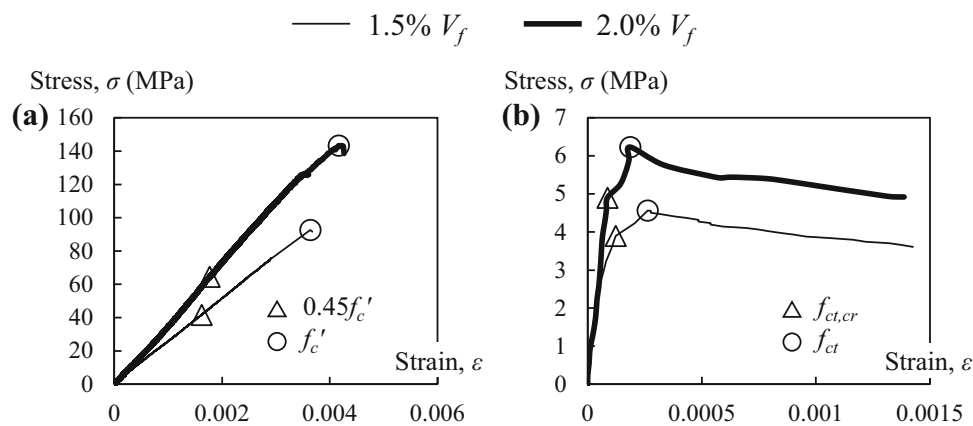
Fig. 3 Stress–strain curves of UHPFRC: **a** compression test result and **b** tension test result.

$0.45f_{cu}$, ACI 318-14) were 92.6 MPa and 25.7 GPa for the 1.5% V_f UHPFRC, respectively, or 143.3 MPa and 36.5 GPa for the 2.0% V_f UHPFRC. The strain (ε_{co}) at peak stress was approximately 0.004. The UHPFRC also showed quite large tensile strength and ductility. As shown in Fig. 3(b), the tensile behavior was also nearly linear-elastic up to the first cracking ($f_{ct,cr}$), followed by gradual strain-softening after reaching peak stress (tensile strength f_{ct} = 4.56 MPa and tensile strain ε_{ct} = 0.00026 for the 1.5% V_f UHPFRC, or f_{ct} = 6.23 MPa and ε_{ct} = 0.00020 for the 2.0% V_f UHPFRC). Such a desirable tensile behavior was achieved by the interaction of steel fibers in the microscopic level and their ability to sustain loads after the onset of cracking. It is noted that the mechanical properties of UHPFRC used in the present study were lower than those specified in AFGC (Toutlemonde and Resplendino 2011): compressive strength greater than 150 MPa, elastic modulus around 50 GPa, and tensile strength higher than 7 MPa. The lower mechanical properties may be attributed to insufficient mixing and initial curing before thermal treatment. Further research is required on the lower mechanical properties.

For the NSC core, ready-mixed concrete was used, resulting in f_{cu} = 28.2 MPa and E_c = 21.5 GPa.

2.2.2 Reinforcement

Direct tension tests for reinforcing bars were carried out according to ASTM E8-09 (2009). Table 3 summarizes the mechanical properties of the reinforcement. The modulus of elasticity (E_s), yield strength (f_y), and ultimate (tensile) strength (f_u) on average were 218 GPa, 382 MPa, and 537 MPa, respectively, for 10 mm-diameter transverse bars. For 22 mm-diameter longitudinal bars, E_s = 228 GPa, f_y = 263 MPa, and f_u = 417 MPa. For 16 mm-diameter threaded bars, E_s = 182 GPa, f_y = 398 MPa, and f_u = 508 MPa.

2.3 Production of Column Specimens

Because the wall thickness of the UHPFRC tube was very thin, each UHPFRC tube was produced by sequential concrete placements rotating the section (Kim et al. 2016). Figure 4 shows the production sequence: (1) a pair of UHPFRC panels (Face1 and Face2) were prepared by casting concrete on the ground (Fig. 4a: except HCC5, a wire-mesh was embedded in each panel, and the inner surface of each panel was roughened before concrete-setting for better bond with the third and fourth panels and concrete core); (2) after rotating the two panels to the opposite faces of the section (90°, Fig. 4b), concrete was poured for the third

Table 3 Measured mechanical properties of reinforcement.

Nominal diameter (mm)	Nominal area (mm²)	Modulus of elasticity (GPa)	Yield strength (MPa)	Yield strain (mm/mm)	Ultimate strength (MPa)
10 (trans. bars)	78.54	218.02	381.97	0.00176	536.66
22 (longi. bars)	380.13	228.26	263.07	0.00115	416.63
16 (threaded bars)	201.06	182.18	397.89	0.00218	508.07
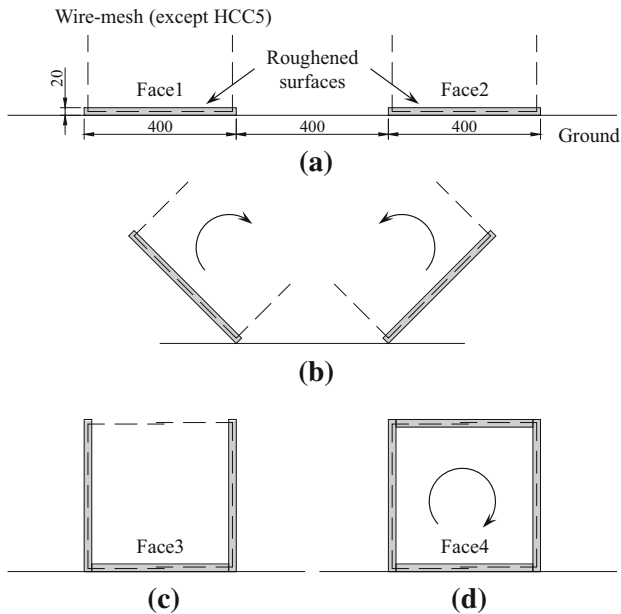
Fig. 4 Production sequence of UHPFRC tube (units: mm): **a** Step1 (Face1 and Face2), **b** Step2 (90° rotation), **c** Step3 (Face3), and **d** Step4 (180° rotation, Face4).

panel (Face3) between the two side panels (Fig. 4c); and (3) after a 180-degree rotation, concrete was poured for the fourth panel (Face4) to form a UHPFRC tube (Fig. 4d).

After each production step, the UHPFRC panels were steam-cured at an elevated temperature of 100 °C (total 48 h), and then the completed UHPFRC tubes were kept at room temperature. About 7 days after the completion, the UHPFRC tubes were erected and then their cores were filled with NSC. Transverse, longitudinal, and threaded bars were placed prior to core-filling.

2.4 Test Setup and Instrumentation

Figure 5 shows the test setup and instrumentation. Concentric axial load tests were performed using a 5 MN compression testing machine, with loading applied only to the NSC core. To this end, a set of rigid steel plates for loading (same in size with the core) was positioned at column ends. To avoid any eccentricity, each column specimen was adjusted in such a way that the center line of axial loading coincides with the longitudinal axis of the column, and to ensure the complete contact with the loading plates, the top and bottom end surfaces of each column specimen were leveled with a layer of high-strength plaster powder.

The column specimens were tested under both load and deformation controls: (1) compression loading was applied at an average rate of 1 kN/sec up to the level of 70% of the expected peak load; (2) at this point, the loading rate was changed to 0.5 kN/s until the peak load was reached; (3) in the softening branch, loading was switched to deformation control with a rate of 0.2 mm/s; and (4) testing was terminated when the post-peak load was decreased to 75% of the peak load.

Eight linear variable differential transducers (LVDTs) were installed to measure relative displacements (during testing, LVDTs were carefully monitored to prevent any accidental eccentricity), with four between the top and bottom loading plates and the other four at the mid height of each specimen. To measure strains, sixteen strain-gauges were installed on concrete and transverse bars (Fig. 5; four on mid-height UHPFRC surfaces, two on UHPFRC joint surfaces, eight on UHPFRC surfaces beneath embedded threaded bars, and two on mid-height transverse bars).

3. Test Results

3.1 Failure Mode

Figure 6 shows the failure mode of the column specimens at the end of testing. As the axial load increased, vertical cracks developed along the UHPFRC tube joints (joint-cracks between the UHPFRC panels) and gradually grew wider under further loading. On the other hand, cracks developing within the UHPFRC panels were relatively minor, because steel fibers restricted the growth of cracks. Around the peak load, there were notably loud sounds associated with localized debonding between the structural components, followed by the failure of steel fibers and wire-mesh and crushing of concrete. Finally, wide vertical, horizontal, and/or diagonal cracks were observed in the middle of the UHPFRC panels (middle-cracks around embedded threaded bars), and the UHPFRC tube was delaminated from the NSC core at a large displacement. The middle-cracks were more obvious at the upper and lower parts of the column. The following three causes appeared to be responsible for these joint-cracks and delamination: (1) load transfer at the interface between the UHPFRC tube and NSC core; (2) insufficient integrity between the UHPFRC panels; and (3) buckling of longitudinal bars at the corner locations. On the other hand, the bearing of embedded threaded bars was responsible for the middle-cracks.
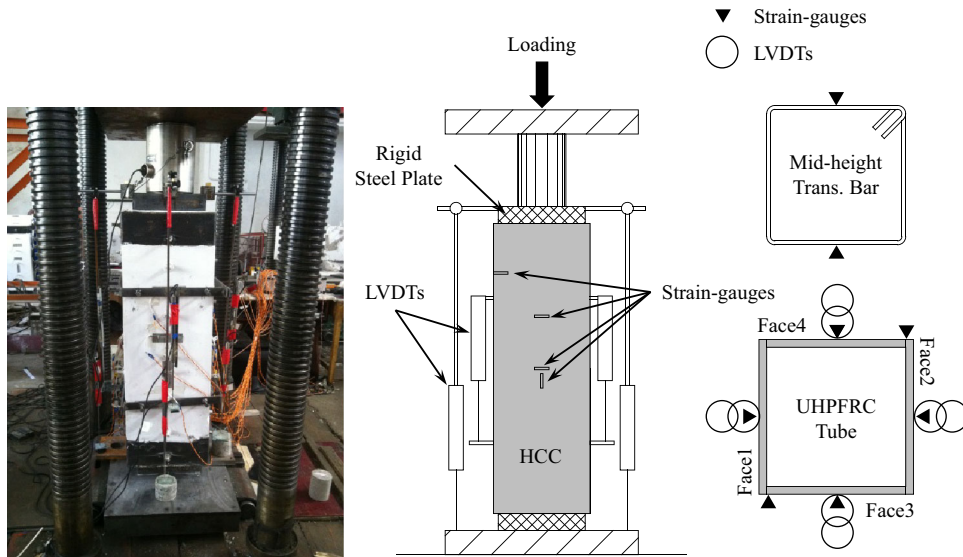
Fig. 5 Test setup and instrumentation.

3.2 Crack Patterns

The crack patterns of each column specimen on four faces are also presented in Fig. 6. To identify the development and propagation of cracks, each crack is plotted with a sequence number, and the wide cracks resulting from local failure are plotted using bold lines. In Table 4, the cracking sequences for all the column specimens are summarized depending on the load level.

More specifically, in the control specimen HCC1 (Fig. 6a), the first crack developed along a UHPFRC joint (on Face4) under the axial load of 2190 kN, and similar vertical cracks were observed on the opposite side (Face3). Hairline cracks then appeared within the UHPFRC panels. Under further loading, crushing cracks appeared around the embedded threaded bars due to bearing. Subsequently, wide vertical and horizontal cracks between the embedded threaded bars were caused by the bearing and outward bulging of the NSC core.

In HCC2 with the greater fiber fraction (Fig. 6b), crack patterns were generally similar to HCC1, but the first crack occurred in a later phase (under 2416 kN) than in HCC1. Cracks were well distributed over the column length. In HCC3 with the lower transverse bar ratio (Fig. 6c), the first crack occurred much earlier under 2084 kN, and the vertical cracks in the middle of UHPFRC panels were more pronounced compared to HCC1 with the higher transverse bar ratio. In HCC4 with the greater fiber content and lower transverse bar ratio (Fig. 6d), the first crack occurred under 2351 kN, similarly to HCC2. This is a later phase than in the control specimen HCC1. In HCC5 without wire-mesh (Fig. 6e), the first crack occurred under the smallest load of 2100 kN and the vertical cracks in the middle of UHPFRC panels were most severe. Additionally, a wide diagonal crack extending from the upper left corner to the mid-height of the column was also observed.

The crack patterns showed that (1) the provided steel fibers were effective in delaying the middle-cracks; and (2)

the wire-mesh embedded in the UHPFRC panels was effective to keep the joint-cracks tightly closed. However, in the case of using the sequential concrete placement method (or rotation method), the vertical cracks along the UHPFRC tube joints (or joint-cracks) were critical to the overall performance. Thus, in order to ensure the better performance, the UHPFRC tube needs to be monolithically constructed.

3.3 Axial Load–Displacement Relationship

Figure 7 shows the axial load–displacement curves ($P–\delta$) of the column specimens. The axial displacement (δ) indicates the change in vertical length between column ends. In the figure, vertical large-dashed lines represent the yield displacement (δ_y, defined as the yield displacement of an equivalent elastoplastic system with the secant stiffness at 75% of the peak load (Park 1989); see Fig. 8) and ultimate displacement (δ_u, defined as the post-peak displacement corresponding to 80% of the peak load (Park 1989); see Fig. 8), and circle marks indicate the measured loads (P_{cr} and P_p) at the first cracking and peak, respectively. All the curves are plotted together in Fig. 7(f) for comparison, and the test results are summarized in Tables 5 and 6. In the figure, two bilinear small-dashed curves indicate the predictions by ACI 318-14, and solid triangle marks with P_b indicate the design bearing strength. The predictions by ACI 318-14 and design bearing strength will be discussed in the next section.

In the control specimen of HCC1 (V_f = 1.5%, s = 100 mm, and wire-mesh), the axial load increased linearly up to the first cracking at P_{cr} = 2190 kN and δ_{cr} = 0.7 mm. After reaching the peak load (P_p) of 3369 kN at δ_p = 2.6 mm, the axial load gradually decreased. The initial stiffness (k_i) was 3466 kN/mm, where the nominal elastic stiffness or slope of the curve was defined as the secant stiffness at $0.45P_p$. The displacement ductility was estimated as $\mu = \delta_u/\delta_y = 3.3$, where the ultimate displacement (δ_u) was 4.3 mm.
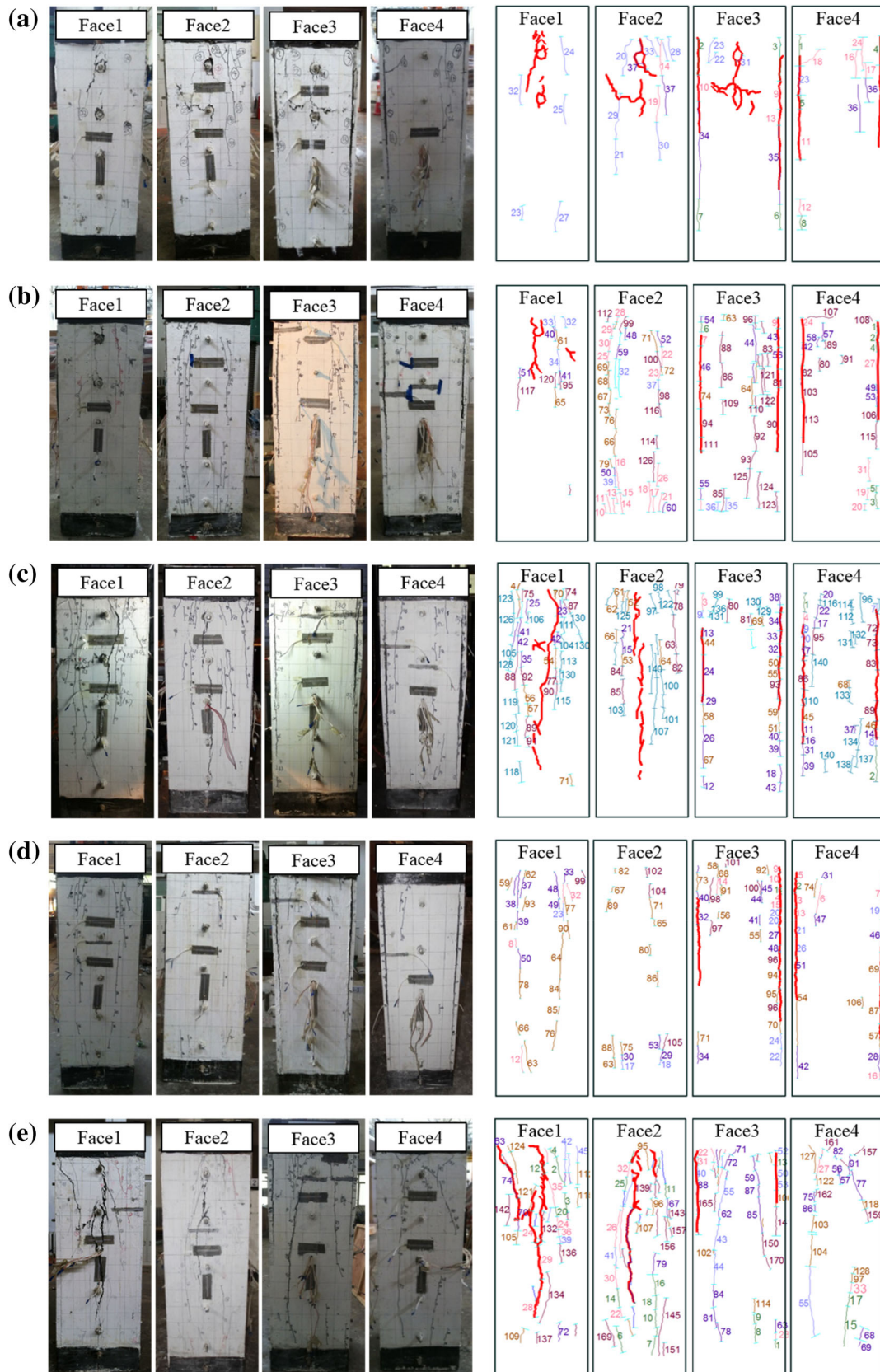
Fig. 6 Failure modes and crack patterns of column specimens: **a** HCC1 (control: V_f = 1.5%, s = 100 mm, wire-mesh), **b** HCC2 (V_f = 2.0%), **c** HCC3 (s = 200 mm), **d** HCC4 (V_f = 2.0%, s = 200 mm), and **e** HCC5 (no wire-mesh).

In the HCC2 specimen (V_f = 2.0%), the use of the greater fiber fraction in the UHPFRC tube resulted in increases of the initial stiffness (k_i = 3776 kN/mm or 109% of HCC1) and peak load (P_p = 3729 kN or 111% of HCC1), though the displacement ductility was similar (μ = 3.2, δ_u = 4.0 mm). In the HCC3 specimen with the larger s (200 mm) but with the same V_f (1.5%), the peak load was unexpectedly higher (P_p = 3440 kN or 102% of HCC1) than in HCC1, but

Table 4 Description of cracking sequences.

HCC1 (control)		HCC2 (V_f = 2.0%)		HCC3 (s = 200 mm)		HCC4 (V_f = 2.0%, s = 200 mm)		HCC5 (no wire-mesh)	
Crack no.	Load range (kN)	Crack no.	Load range (kN)	Crack no.	Load range (kN)	Crack no.	Load range (kN)	Crack no.	Load range (kN)
1–8	2100–2400	1–6	2400–2700	1–2	2000–2200	1–2	2300–2600	1–20	2100–2400
9–19	2400–2700	7–31	2700–2900	3–5	2200–2400	3–16	2600–2800	21–37	2400–2600
20–33	2700–3000	32–39	2900–3100	6–10	2400–2600	17–26	2800–3000	38–55	2600–2800
34–37	3000–3100	40–60	3100–3300	11–43	2600–2800	27–53	3000–3200	56–94	2800–3000
NM	3100–	61–79	3300–3500	44–71	2800–3000	54–95	3200–3500	95–129	3000–3200
		80–126	3500–3700	72–95	3000–3200	96–106	3500–3600	130–173	3200–3300
		NM	3700–	96–140	3200–3400	NM	3600–	NM	3300–
				NM	3400–				

NM not measured due to safety concern.
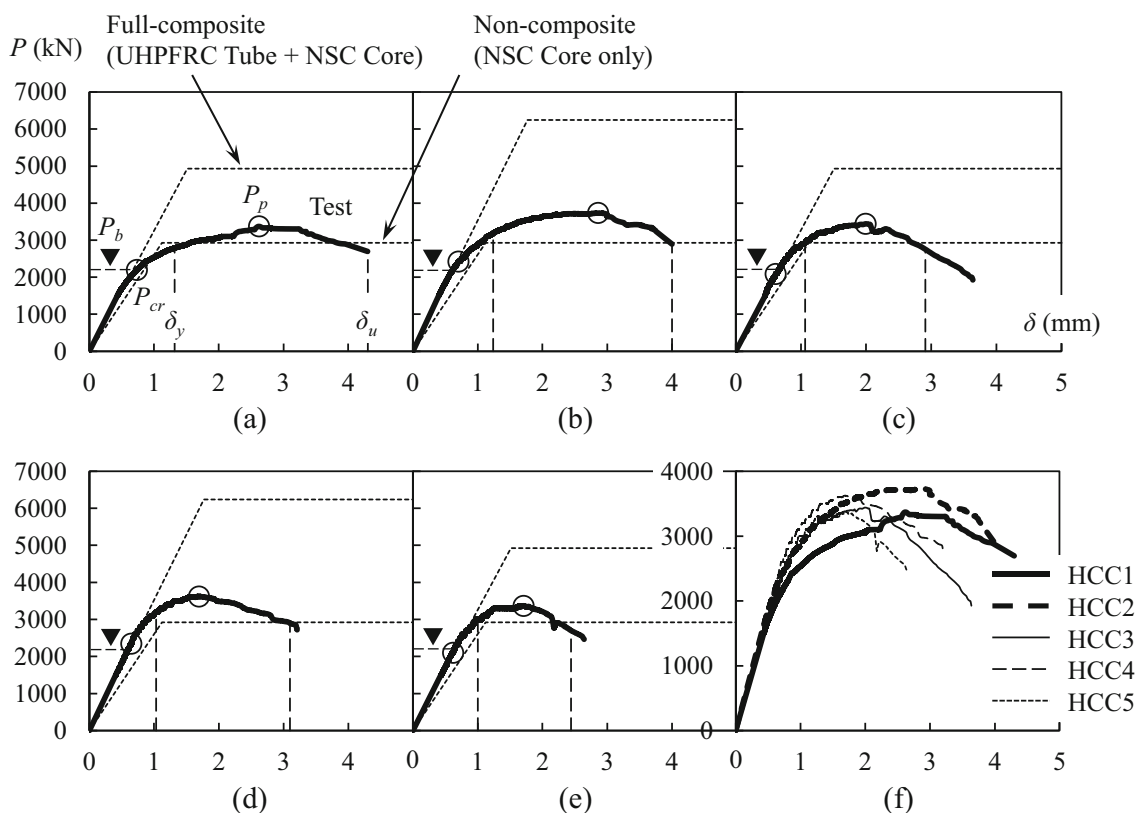
Fig. 7 Axial load–displacement relationship of column specimens: **a** HCC1 (control), **b** HCC2 (V_f = 2.0%), **c** HCC3 (s = 200 mm), **d** HCC4 (V_f = 2.0%, s = 200 mm), **e** HCC5 (no wire-mesh), **f** comparison.

the increase was marginal and the ductility was much lower (μ = 2.7, δ_u = 2.9 mm). In the specimen HCC4 with the larger s (200 mm) and V_f (2.0%), the initial stiffness was higher with 3689 kN/mm (or by 6%) and the peak load was higher with 3624 kN (or by 8%), but the ductility was lower as 3.0 (or by 10%), compared to HCC1. Although the UHPFRC tube was indirectly loaded by bearing of threaded bars, the positive effect of the fiber fraction in the UHPFRC tube on the axial load behavior of the hybrid concrete column can be observed by comparing the performance

between HCC3 and HCC4 and between HCC1 and HCC2 (see Tables 5 and 6).

In HCC5 without wire-mesh, the initial stiffness and peak load (k_i = 3476 kN/mm and P_p = 3370 kN) were similar to HCC1. However, the post-peak behavior was not so ductile (μ = 2.4, δ_u = 2.4 mm). This is clearly presented in Fig. 7(f), where all the axial load–displacement curves are plotted for comparison. This was due to early buckling of longitudinal bars at corners, where the structural integrity between the UHPFRC panels was poor. Thus, the steel wire-

mesh embedded in the UHPFRC tube is essential for the ductile behavior of the developed hybrid concrete columns.

In conclusion, the axial load behavior of the column specimens varied greatly with the test parameters. The different behavior was partly attributed to the contribution of the UHPFRC tube, which was not directly loaded but indirectly. The contribution of the UHPFRC also can be observed in Fig. 9, where the strain of transverse bars at the mid-height is plotted (yield strain of the transverse bars $\varepsilon_{yt} = f_{yt}/E_{st} = 0.0018$). As shown in the figure, the transverse bars of HCC2 and HCC4 ($V_f = 2.0\%$) yielded before the peak load, indicating that the axial load increased even after the yielding of transverse bars. In contrast, the transverse bars of HCC1 or HCC3 ($V_f = 1.5\%$) yielded after the peak load or did not yield at all. This is because the peak load of the HCC column was developed by the combined effect of the confinement of transverse bars (exerting on the NSC core) and the contribution of the UHPFRC tube (related to the steel fiber content). In HCC5, strain-gauges were
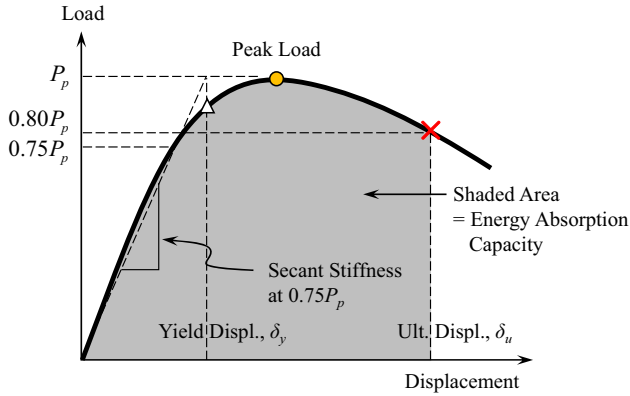
Fig. 8 Definitions of yield displacement, ultimate displacement, and energy absorption capacity.
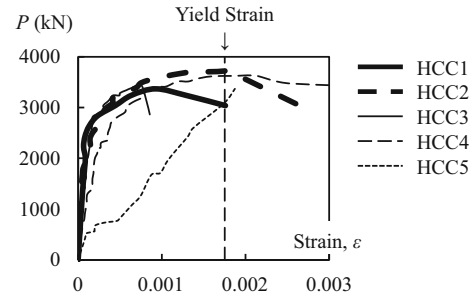
Fig. 9 Strains of transverse reinforcement.

Table 5 Test results.

Specimen	1st crack		Yield displacement		Peak load		Ultimate displacement	
	P_{cr} (kN)	δ_{cr} (mm)	P_y (kN)	δ_y (mm)	P_p (kN)	δ_p (mm)	P_u (kN)	δ_u (mm)
HCC1 (control)	2190	0.7	2787	1.3	3369	2.6	2695	4.3 (3.3)
HCC2 ($V_f = 2.0\%$)	2416	0.7	3194	1.2	3729	2.9	2893	4.0 (3.2)
HCC3 ($s = 200$ mm)	2084	0.6	2944	1.1	3440	2.0	2754	2.9 (2.7)
HCC4 ($V_f = 2.0\%$, $s = 200$ mm)	2351	0.6	3199	1.0	3624	1.7	2899	3.1 (3.0)
HCC5 (no wire-mesh)	2100	0.6	3003	1.0	3370	1.7	2700	2.4 (2.4)

P = load, δ = displacement, and in parenthesis = displacement ductility ($\mu = \delta_u/\delta_y$).

Table 6 Comparison of test results with predictions by design code.

Specimen	Test results[a]		Predictions by design code[b]			
			Non-composite (NSC core only)		Full-composite (UHPFRC Tube + NSC core)	
	k_i (kN/mm)	P_p (kN)	k_e (kN/mm)	P_o (kN)	k_e (kN/mm)	P_o (kN)
HCC1 (control)	3466	3369	2610	2926	3262	4930
HCC2 ($V_f = 2.0\%$)	3776	3729	2610	2926	3534	6241
HCC3 ($s = 200$ mm)	3318	3440	2610	2926	3262	4930
HCC4 ($V_f = 2.0\%$, $s = 200$ mm)	3689	3624	2610	2926	3534	6241
HCC5 (no wire-mesh)	3476	3370	2610	2926	3262	4930

[a]For test results, initial stiffness $k_i = P/\delta$ was defined at $0.45P_p$.
[b]For predictions by design code, elastic stiffness k_e and axial strength P_o were determined by Eqs. (1a) and (2a) using converted cylinder strength.

damaged by concrete crushing and cracking, thus the measured strains cannot be employed in this case.

4. Discussion

4.1 Contribution of UHPFRC Tube

Even though the UHPFRC tube was not directly loaded, the contribution of the UHPFRC on the axial behavior was substantial. The behavior was primarily dependent upon the degree of composition, which was affected by the bearing strength of the bar-tube interfaces. To better examine the contribution of the UHPFRC tube, the measured initial stiffness (k_i) and peak load (P_p) were compared with the predictions obtained from ACI 318-14. Under concentric axial compression, the design elastic stiffness (k_e) and nominal axial strength (P_o) can be predicted using Eqs. (1a) and (2a), respectively, where the subscript 1 or 2 indicates the non-composite (NSC core only) or full-composite section (NSC core and UHPFRC tube).

$$k_{e,1} = \frac{(E_c A_c)_{\text{NSC}} + (E_s A_s)}{L} \tag{1a}$$

$$k_{e,2} = \frac{(E_c A_c)_{\text{NSC}} + (E_c A_c)_{\text{UHPFRC}} + (E_s A_s)}{L} \tag{1b}$$

$$P_{o,1} = 0.85 (f'_c A_c)_{\text{NSC}} + (f_y A_s) \tag{2a}$$

$$P_{o,2} = 0.85 \left[(f'_c A_c)_{\text{NSC}} + (f'_c A_c)_{\text{UHPFRC}} \right] + (f_y A_s) \tag{2b}$$

where E_c = modulus of elasticity of concrete (NSC or UHPFRC), E_s = modulus of elasticity of longitudinal bars, A_c = cross-sectional area of concrete (NSC or UHPFRC), A_s = cross-sectional area of longitudinal bars, L = column length, f'_c = specified compressive strength of concrete (NSC or UHPFRC), and f_y = specified yield strength of longitudinal bars.

It is noted that, to take into account the size effect (Graybeal and Davis 2008; Neville 2011) in the predictions, the cube strength was converted to the cylinder strength based on the strength class conformity of Eurocode 2-04 (2004a): specific cylinder-to-cube strength ratios for strength classes up to C55/67 and a constant difference of 15 MPa for higher strength classes (Tam et al. 2017). The converted cylinder strength (f'_c) was 77.6, 128.3, or 23.2 MPa for the 1.5% V_f UHPFRC, 2.0% V_f UHPFRC, or NSC.

Equations (1a) and (2a) give the upper and lower bounds of the actual behavior, that is, the axial load capacities for the full-composite section (consisting of the UHPFRC tube and in-filled NSC core) and for the non-composite section (NSC core only), respectively. The two bounds are summarized in Table 6 and also plotted using two bilinear curves in Fig. 7, which include the information of k_e and P_o. As shown, the axial load behavior generally corresponded to the upper bound at the initial loading stage and to the lower bound beyond the bearing failure of the embedded threaded bars. The design bearing strength (P_b) can be predicted by

Eurocode 4-04 (2004b), as given in Eq. (3a) for threaded bar failure and Eq. (3b) for UHPFRC panel failure.

$$P_b = \sum \left(0.8 f_u \frac{\pi d^2}{4} \right)_{\text{threaded bars}} \tag{3a}$$

$$P_b = \sum \left(0.29 d^2 \sqrt{f'_c E_c} \right)_{\text{UHPFRC}} \tag{3b}$$

where f_u = tensile strength of a threaded bar, d = diameter of a threaded bar, f'_c = specified compressive strength of UHPFRC, and E_c = modulus of elasticity of UHPFRC.

Because threaded bars were placing passing through all 4 faces and with 7 levels over the column height, the total bearing strength was calculated by the smaller of the values obtained from Eqs. (3a) and (3b) multiplied by 28. As shown by the triangular marks in Fig. 7, the predicted value by Eqs. (3a) and (3b) (P_b) was 2288 kN for the specimens with both 1.5 and 2.0% fiber volume fractions, because it was governed by the failure of threaded bars. This predicted value agreed quite well with the actual onset of the observed bearing failure.

Even after the bearing failure at the bar-tube interfaces, the larger peak load was obtained compared with the lower bound prediction. This is mainly due to the confinement provided by transverse bars. However, the UHPFRC tube also had a contribution to the axial load capacity. Figure 10 demonstrates the contribution of UHPFRC tube. The thin dotted curves in Fig. 10 was obtained for the confined NSC core only using the numerical method developed by Kim et al. (2012) which accounts for the confinement effect quite accurately. As shown in the figure, the HCC specimens had the higher strength than the analysis results for the confined NSC core only, indicating the presence of the UHPFRC tube contribution even after the onset of the bearing failure. The higher strength was not caused by the confinement effect of the UHPFRC tube: the confinement effect of the UHPFRC tube cannot be expected to be as high as that of transverse bars, because the tensile strain of UHPFRC was much lower than the yield strain of transverse bars and also the UHPFRC tube was subjected to axial load, even though the geometrical effectiveness of the UHPFRC tube (continuous along the column height) was better than transverse bars (intermittently spaced). As shown in Fig. 6, the bearing failure did
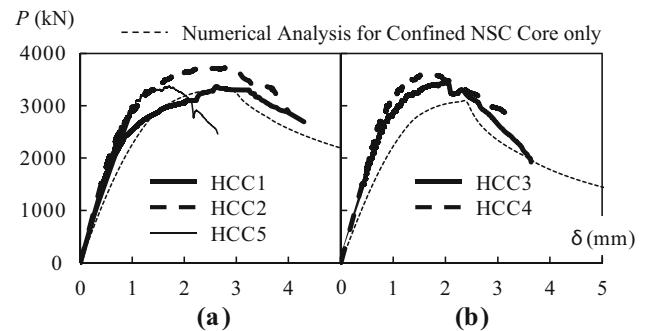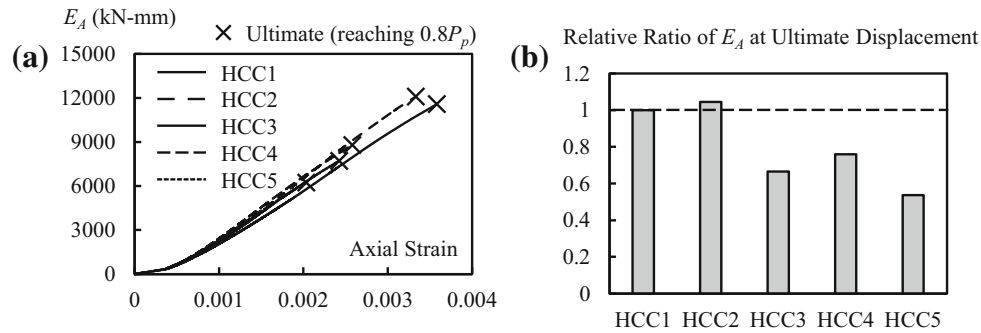

Fig. 10 Comparison of test results with numerical analysis for confined NSC core only: **a** s = 100 mm and **b** s = 200 mm.

Fig. 11 Energy absorption capacities of column specimens: **a** axial strain–energy dissipation relationship and **b** comparison of energy dissipation at ultimate displacement.

not occur at the whole bar-tube interfaces, because the NSC core was compressed by the top and bottom loading plates together. The threaded bars around the mid-height underwent the smaller deformation than the upper and lower threaded bars. Thus, the UHPFRC tube did not completely lose its contribution to the axial load capacity (by bearing) until its full delamination at a large deformation. Because the same threaded bars were used, the difference in peak load was attributed to the contribution of the UHPFRC tube, which was related to the steel fiber content.

In this comparison, it is also observed that the initial stiffness of all the test specimens was larger than the analysis results for the NSC core only, demonstrating that the composite action would be effective at the service loading stage.

4.2 Energy Absorption Capacity

For more quantitative assessment of the effect of the test parameters, energy absorption capacities were compared. The energy absorption capacity (E_A) is defined as the area under the axial load–displacement curve up to the ultimate displacement (shaded area in Fig. 8), as expressed using the following equation.

$$E_A = \int_0^{\delta_u} P d\delta \tag{4}$$

Figure 11 shows the energy absorption capacity of the column specimens. As shown in Fig. 11a, the accumulative energy absorption capacity was increased with the axial strain, due to the strength development and displacement ductility. Figure 11b compares the accumulative energy absorption capacity at the ultimate displacement. Compared with the control specimen HCC1 ($E_A = 11,578$ kN mm), HCC2 with the greater fiber fraction ($E_A = 12,093$ kN mm) showed the higher energy dissipation by 4%. However, the energy dissipation was markedly decreased by 33% in HCC3 with the lower transverse bar ratio ($E_A = 7706$ kN mm) or by 24% in HCC4 with the greater fiber fraction and lower transverse bar ratio ($E_A = 8796$ kN mm). On the other hand, HCC5 without wire-mesh ($E_A = 6220$ kN mm) showed the lowest energy dissipation (decreased by 46%) due to early buckling of longitudinal bars. The transverse bar ratio is shown to be the most influential parameter among the tested parameters in terms of the energy dissipation. On the other hand, the indirectly loaded UHPFRC tube had a limited influence, but the structural integrity of the UHPFRC tube appeared to affect the restraining of bar-buckling, which could result in a reduction of the energy dissipation.

5. Conclusions

To investigate the axial load behavior of HCC consisting of a UHPFRC tube (20 mm thick, 92.6 or 143.3 MPa) and NSC core (28.2 MPa), concentric axial load tests were performed for five HCC. Axial loading was applied to the NSC core only, and the UHPFRC tube was indirectly loaded by bearing of embedded threaded bars. Test parameters included the volume fraction of steel fibers, volumetric ratio of transverse bars, and usage of wire-mesh in the UHPFRC tube. The conclusions from the experimental investigation are summarized as follows:

(1) In terms of sectional and cost efficiencies, the use of UHPFRC only in the perimeter of a cross-section is beneficial (i.e., hybrid concrete columns with different strengths in the concrete cover and concrete core), because the UHPFRC has high strength both in compression and tension, toughness, and durability and can also function as a permanent form. The feasibility of the system discussed was demonstrated by structural tests of axially loaded column specimens.

(2) The axial load behavior of the hybrid column specimens, such as cracking, initial stiffness, peak load, displacement ductility, and energy absorption capacity, varied greatly with the test parameters. Generally, as the steel fiber fraction increased or the transverse bar ratio increased, the axial stiffness, strength, ductility, and energy absorption capacity were favorable. The presence of wire-mesh primarily affected bar-buckling and post-peak behavior.

(3) The axial load behavior corresponded to the upper bound of full-composite action between the UHPFRC tube and NSC core at the stage of initial loading, and then corresponded to the lower bound of non-composite action of the NSC core only after the bearing failure of embedded threaded bars. The onset of the bearing failure agreed quite well with the design bearing strength predicted by Eurocode 4.

(4) In the present study, the thin UHPFRC tube was produced by sequential concrete placements rotating the section, and there were many vertical cracks observed at the corner cold joints. In the future, to improve the overall structural integrity, hollow-core UHPFRC tubes may be made by monolithic casting.

Further research on the hybrid concrete columns with the permanent UHPFRC tubing form should be continued, particularly regarding the behavior of slender hybrid concrete columns with the UHPFRC tube under eccentric axial loads as well as cyclic loads.

Acknowledgements

Author Contributions

All of the authors contributed critically to conception, design, test, and analysis as well as drafting and revision of the manuscript.

Conflict of interest

The authors declare that they have no conflict of interest.

Open Access

References

American Concrete Institute. (2014). *Building Code Requirements for Structural Concrete and Commentary (ACI 318-14)*. Farmington Hills, MI: American Concrete Institute.

American Society for Testing and Materials (ASTM). (2009). *Standard Test Methods for Tension Testing of Metallic Materials (ASTM E8-09)*. West Conshohocken, PA: American Society for Testing and Materials (ASTM).

American Society for Testing and Materials (ASTM) (2011) Standard Test Method for Compressive Strength of Hydraulic Cement Mortars (Using 2-in. or [50 mm] Cube Specimens) (ASTM C109-11). West Conshohocken, PA.

Association Française de Génie Civil (AFGC) (2002) Ultra High Performance Fibre-Reinforced Concretes—Interim Recommendations, Paris, France

Collins, M. P., Mitchell, D., & MacGregor, J. G. (1993). Structural design considerations for high-strength concrete. *Concrete International: Design and Construction, 15*(5), 27–34.

Cusson, D., & Paultre, P. (1994). High-strength concrete columns confined by rectangular ties. *Journal of Structural Engineering, ASCE, 120*(3), 783–804.

European Committee for Standardization (CEN) (2004a) Design of Concrete Structures—Part 1-1: General Rules and Rules for Buildings (Eurocode 2-04). Brussels.

European Committee for Standardization (CEN) (2004b) Design of Composite Steel and Concrete Structures—Part 1-1: General Rules and Rules for Buildings (Eurocode 4-04). Brussels.

Fehling, E., Schmidt, M., & Stürwald, S. (2008) Ultra High Performance Concrete (UHPC). *Proceedings of the Second International Symposium on Ultra High Performance Concrete*. Kassel, Germany, No. 10.

Foster, S. J., & Mario, M. A. (2001). Strength and ductility of fiber-reinforced high-strength concrete columns. *Journal of Structural Engineering, ASCE, 127*(1), 28–34.

Graybeal BA (2006) Material Property Characterization of Ultra-High Performance Concrete. Federal Highway Administration Report No. FHWA-HRT-06-103, 186 pp.

Graybeal, B., & Davis, M. (2008). Cylinder or cube: Strength testing of 80–200 MPa (11.6–29 ksi) ultra-high-performance fiber-reinforced concrete. *ACI Materials Journal, 105*(6), 603–609.

Graybeal, B. A., Hartmann, J. L. (2003). Strength and durability of ultra-high performance concrete. *Concrete Bridge Conference*. Portland Cement Association.

Japan Society of Civil Engineers (JSCE) (2008). Recommendations for Design and Construction of HPFRCC with Multiple Fine Cracks.

Kim, C. S., Lee, H. J., Park, C. K., Hwang, H. J., & Park, H. G. (2017). Cyclic loading test for concrete-filled hollow precast concrete columns produced by using a new fabrication method. *Journal of Structural Engineering, ASCE, 143*(4), 04016212-1-13.

Kim, C. S., Lim, W. Y., Park, H. G., & Oh, J. K. (2016). Cyclic loading test for cast-in-place concrete-filled hollow precast concrete columns. *ACI Structural Journal, 113*(2), 205–215.

Kim, C. S., Park, H. G., Chung, K. S., & Choi, I. R. (2012). Eccentric axial load testing for concrete-encased steel columns using 800 MPa steel and 100 MPa concrete. *Journal of Structural Engineering, ASCE, 138*(8), 1019–1031.

Koo, I. Y., & Hong, S. G. (2016). *Strengthening RC columns with ultra high performance concrete*. Jeju: The 2016 Structures Congress (Structures 16).

Mehta, P. K., & Monteiro, P. J. M. (2006). *Concrete: Microstructure, Properties, and Materials* (3rd ed.). New York: McGraw-Hill.

Mirmiran, A., & Mohsen, S. (1997). Behavior of concrete columns confined by fiber composites. *Journal of Structural Engineering, ASCE, 123*(5), 583–590.

National Standard of People's Republic of China (2003) Standard for Test Method of Mechanical Properties on Ordinary Concrete (GB/T 50081-2002). Beijing, China. (in Chinese)

Nematollahi, B., Saifulnaz, R., Jaafar, M. S., & Voo, Y. L. (2012). A review on ultra-high performance 'ductile' concrete (UHPdC) technology. *International Journal of Civil and Structural Engineering, 2*(3), 1003–1018.

Neves, R. D., & Fernandes de Almeida, J. C. O. (2005). Compressive behaviour of steel fibre reinforced concrete. *Structural Concrete, 6*(1), 1–8.

Neville, A. M. (2011). *Properties of Concrete* (5th ed.). New Jersey: Prentice Hall.

Park, R. (1989). Evaluation of ductility of structures and structural assemblages from laboratory testing. *Bulletin of the New Zealand National Society for Earthquake Engineering, 22,* 155–166.

Park, C. W., Kim, Y. J., Choi, E. S., & Kim, S. W. (2016). Fundamental properties and mechanical characteristics of high performance cement composite with steel fibres under high temperature. *Journal of Structural Integrity and Maintenance, 1*(4), 189–196.

Paultre, P., Eid, R., Langlois, Y., & Lévesque, Y. (2010). Behavior of steel fiber-reinforced high-strength concrete columns under uniaxial compression. *Journal of Structural Engineering, ASCE, 136*(10), 1225–1235.

Pimienta, P. & Chanvillard, G. (2005) Durability of UHPFRC specimens kept in various aggressive environments. *10DBMC International Conference on Durability of Building Materials and Components*. Lyon, France, TT3-246.

Shanmugapriya, T., & Uma, R. N. (2013). Experimental investigation on silica fume as partial replacement of cement in high performance concrete. *The International Journal of Engineering and Science, 2*(5), 40–45.

Tam, C. T., Daneti, S. B., & Li, W. (2017). EN 206 conformity testing for concrete strength in compression. *Procedia Engineering, 171,* 227–237.

Toutlemonde F, Foure B, Sorelli L, Baby F, Marchand P, Ulm FJ (2000) An overview of research advances from 2002 concerning UHPFRC, in view of updating AFGC recommendations. *Proceedings of the International Workshop on UHPFRC*. Marseille, France, Paper 5.3.4.

Toutlemonde, F., & Resplendino, J. (2011). *Designing and Building with UHPFRC: State of the Art and Development*. New Jersey: Wiley.

Tsonos, A. G. (2009). Ultra-high-performance fiber reinforced concrete: an innovative solution for strengthening old R/C structures and for improving the FRP strengthening method. Computational Methods and Experiments in Materials Characterisation IV. *WIT Transactions on Engineering Sciences, 64,* 273–284.

Wang, Y. C., & Lee, M. G. (2007). Ultra-high strength steel fiber reinforced concrete for strengthening of RC frames. *Journal of Marine Science and Technology, 15*(3), 210–218.